Role of the C-Terminal Region of the B Component of *Methylosinus trichosporium* OB3b Methane Monooxygenase in the Regulation of Oxygen Activation†

Jingyan Zhang and John D. Lipscomb*

Department of Biochemistry, Molecular Biology, and Biophysics and Center for Metals in Biocatalysis, University of Minnesota, Minneapolis, Minnesota 55455

Received August 26, 2005; Revised Manuscript Received December 7, 2005

ABSTRACT: The effects of the C-terminal region of the B component (MMOB) of soluble methane monooxygenase (sMMO) from *Methylosinus trichosporium* OB3b on steady-state turnover, the transient kinetics of the reaction cycle, and the properties of the sMMO hydroxylase (MMOH) active site diiron cluster have been explored. MMOB is known to have many profound effects on the rate and specificity of sMMO. Past studies have revealed specific roles for the well-folded core structure of MMOB as well as the disordered N-terminal region. Here, it is shown that the disordered C-terminal region of MMOB also performs critical roles in the regulation of catalysis. Deletion mutants of MMOB missing 5, 8, and 13 C-terminal residues cause progressive decreases in the maximum steady-state turnover number, as well as lower apparent rate constants for formation of the key reaction cycle intermediate, compound **Q**. It is shown that this latter effect is actually due to a decrease in the rate constant for formation of an earlier intermediate, probably the hydroperoxo species, compound **P**. Moreover, the deletions result in substantial uncoupling at or before the **P** intermediate. It is proposed that this is due to competition between slow H_2O_2 release from one of the intermediates and the reaction that carries this intermediate on to the next step in the cycle, which is slowed by the mutation. Electron paramagnetic resonance (EPR) studies of the hydroxylase component (MMOH) in the mixed valent state suggest that complexation with the mutant MMOBs alters the electronic properties of the diiron cluster in a manner distinct from that observed when wild-type MMOB is used. Active site structural changes are also suggested by a substantial decrease in the deuterium kinetic isotope effect for the reaction of **Q** with methane thought to be associated with a decrease in quantum tunneling in the C−H bond breaking reaction. Thus, the surface interactions between MMOH and MMOB that affect substrate oxidation and its regulation appear to require the complete MMOB C-terminal region for proper function.

Methane monooxygenase (MMO)[1] catalyzes the NADH-coupled reaction of methane with O_2 to form methanol and water in essentially 100% yield (*1*).

$$NAD(P)H + H^+ + CH_4 + O_2 \rightarrow NAD(P)^+ + CH_3OH + H_2O$$

MMO can also catalyze oxidations of a broad spectrum of organic compounds, which further stimulates interest in its catalytic mechanism and structure (*2*, *3*). The soluble MMO enzymes (sMMO) isolated from *Methylosinus trichosporium* OB3b and *Methylococcus capsulatus* (Bath) have been extensively investigated (*4*−*7*). The enzyme consists of three independent components: an $(\alpha\beta\gamma)_2$, 245 kDa hydroxylase (MMOH) containing a carboxylate- and bis-μ-hydroxo-bridged dinuclear iron center in each protomer, a 38 kDa reductase (MMOR) containing FAD and a [2Fe−2S] cluster, and a 15 kDa regulatory component (MMOB). MMOR provides the two electrons required for catalysis to MMOH, which has been shown to be responsible for O_2 activation and subsequent hydrocarbon oxidation (*8*, *9*).

The reaction cycle of the sMMO system illustrated in Scheme 1 has been proposed on the basis of spectroscopic and transient kinetics studies (*9*−*17*). The resting diferric MMOH is first reduced to diferrous state by reduced MMOR. This state reacts with O_2 to yield the diferrous intermediate **O** in which O_2 is apparently bound to the enzyme but not to the diiron cluster. Intermediate **O** then decays to yield a diferric peroxo or the electronically equivalent mixed-valent superoxo intermediate **P***. **P*** decays to a different diferric peroxo or hydroperoxo species **P**, which exhibits a weak absorption at 700 nm. Intermediate **P** then converts to intermediate **Q**, a unique species that exhibits a relatively intense chromophore at 430 nm. **Q** has been shown to contain a bis-μ-oxo binuclear Fe(IV) cluster that is capable of directly

† This work was supported by the NIH grant GM40466.

* To whom correspondence should be addressed. Mailing address: Department of Biochemistry, Molecular Biology, and Biophysics, 6-155 Jackson Hall, 321 Church St., University of Minnesota, Minneapolis, MN 55455. Telephone: (612) 625-6454. Fax: (612) 624-5121. E-mail: lipsc001@umn.edu.

[1] Abbreviations: MMO, methane monooxygenase; sMMO, soluble form of methane monooxygenase; MMOH, sMMO hydroxylase component; MMOB, sMMO component B; MMOR, sMMO reductase; Quad mutant, MMOB mutant N107G/S109A/S110A/T111A; WT-MMOB, wild-type MMOB; MOPS, 3-[*N*-morpholino]propane-sulfonic acid; $\mathbf{H}^{ox}$, Oxidized MMOH; $\mathbf{H}^{red}$, reduced MMOH.; **O**, **P***, **P**, **Q**, **T**, **T1**; compounds O, P*, P, Q, T, and T1 from the MMOH catalytic cycle.

10.1021/bi051721j CCC: $33.50
Published on Web 01/13/2006

Scheme 1: Proposed Reaction Cycle of sMMO

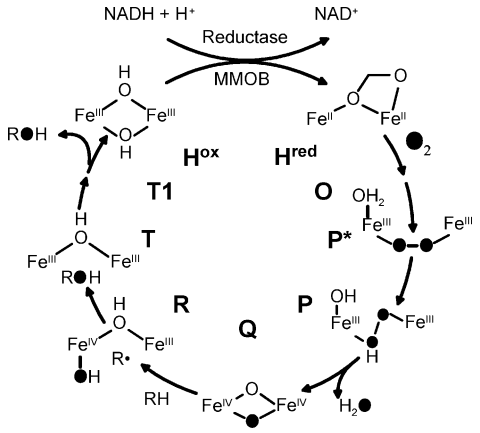

reacting with hydrocarbon substrates to yield the product-bound diferric intermediate **T**. With the release of the product, the resting diferric state MMOH is regenerated in the rate-limiting step of the catalytic cycle.

In the absence of MMOB, sMMO slowly turns over to yield the expected products, but none of the reaction cycle intermediates is observed. This is because O_2 reacts with diferrous MMOH approximately 1000 times faster when MMOB is present, thereby shifting the rate-limiting step from the beginning to the end of the reaction cycle (*15*). Many other remarkable effects of MMOB derive from formation of a specific complex with the α-subunit of MMOH. For example, spectroscopic studies have shown that structural changes are transmitted from the interaction surface to the active site diiron cluster resulting in changes in the cluster environment (*18*−*20*), large shifts in redox potential (*21*, *22*), and alterations in the regiospecificity of hydroxylation of complex substrates (*23*). Mutations in the surface residues of MMOB that interact directly with MMOH have been used to show that it is possible to selectively alter the rate constant for each step in the reaction cycle by using a specific mutant in place of wild-type MMOB (*24*).

The NMR solution structures of MMOB from *Ms. trichosporium* OB3b and *Mc. capsulatus* (Bath) have been solved and provided the basis for identifying the interaction surface of the MMOB−MMOH complex (*25*−*27*). The structures reveal only slight differences between the MMOB proteins from these two sources, so we will focus on the protein from *Ms. trichosporium* OB3b. This protein has a well-folded core (residues 36−126) flanked by N-terminal (residues 1−35) and C-terminal (residues 127−138) regions that possess no significant secondary or tertiary structure in solution. Mutations in the interacting surface of the core domain primarily affect the steps in the reaction cycle in which **Q** reacts with substrates and the products are released (*24*). Kinetic studies of these mutants have revealed what appears to be a major regulatory function of MMOB. Simultaneous mutation of four clustered residues to smaller more hydrophobic residues, to form what is called the Quad mutant, allows large substrates to bind and react more rapidly with **Q**. In addition, large products are released more rapidly from the active site. This suggests that MMOB acts to regulate entry of substrates into the active site of MMOH, perhaps allowing the enzyme to select methane for preferential oxidation on the basis of its size (*24*). Also, the exceptionally large, nonclassical deuterium kinetic isotope effect (KIE) that is observed specifically for the methane reaction with **Q** (*28*) is substantially decreased when the Quad mutant is used (*29*), suggesting that quantum tunneling in the C−H bond breaking reaction is regulated by the MMOH−MMOB interaction.

In addition to the core domain, the disordered N-terminus has been shown to be functionally important (*30*, *31*). Deletion of the N-terminal 29 residues of the *Ms. trichosporium* OB3b MMOB yields a protein that binds to MMOH but does not accelerate the steady-state or single-turnover reactions (*26*). No intermediates in the catalytic cycle are observed with N-terminal deleted MMOB because the formation of **P*** is greatly slowed. Site specific mutations of His33 or His5 in this region to alanine cause large decreases in the rate constants of the **P** or **Q** formation steps of the catalytic cycle, respectively (*24*). Thus, alterations in the N-terminal region primarily affect the steps in the first part of the catalytic cycle that lead to formation of **Q**.

The question considered here is whether the disordered C-terminal region of MMOB is also involved in the interaction between MMOB and MMOH. A series of C-terminal deletions are constructed and their effects on the spectroscopic features of the MMOH diiron cluster and on reaction cycle kinetics are studied. The results show that the MMOB C-terminus is also a key factor in the regulation of sMMO catalysis.

EXPERIMENTAL PROCEDURES

Reagents. All reagents were the highest grade available and purchased from either Sigma (St. Louis, MO) or Aldrich Chemicals (Milwaukee, WI).

Bacterial Growth and Protein Purification. MMOH and MMOR were purified from *Ms. trichosporium* OB3b, and enzyme and protein assays were conducted as previously reported (*8*, *32*). MMOB was purified after overexpression in *E. coli* as previously described (*24*, *25*), but a modified refolding method was used. The cell paste (10−30 g) was suspended in 25 mM MOPS buffer (pH 7), and the cells were broken by French press or sonication. After addition of 1% Triton-X100 and 0.5 mM NaCl, the mixture was stirred at 4 °C for 15 min and then centrifuged at 12 000 × *g* for 30 min. The supernatant was discarded, and the pellet was washed with MOPS buffer and spun for another 10 min. The white pellet was resuspended with 20−50 mL of 8 M urea MOPS buffer, pH 7.0, at room temperature and stirred for 15−30 min to ensure complete denaturation. The insoluble fraction was removed by centrifugation at 5000 × *g* for 10 min. The total protein concentration of the supernatant was determined by Bradford assay. To refold MMOB, the total protein was diluted to 1 mg/mL with 25 mM MOPS buffer, pH 7.0, at a final urea concentration of 1 M. The refolding was carried out at 4 °C with stirring for 30 min followed by centrifugation at 10 000 × *g* for 15 min. The supernatant was then concentrated to ∼50 mL and loaded onto a G-75 column equilibrated with 25 mM MOPS, pH 7.0. The eluted protein was identified by activity assay with MMOH and MMOR, concentrated, and stored at −80 °C.

Site-Directed Mutagenesis. All of the mutations at the C-terminus were made in the pB-WJ400 plasmid (*24*) containing the WT-MMOB gene using a QuickChange kit (Stratagene, La Jolla, CA). All the mutations were confirmed

Table 1: Oligonucleotides Used to Create the MMOB Deletion Mutants

MMOB isoform	Oligonucleotide sequence
Δ126	5'-TTCACCATCACCTAGGAACTCATGGGCCTCGATCGC -3'
	5'-GCGATCGAGGCCCATGAGTTCCTAGGTGATGGTGAA -3'
Δ134	5'-GAACTCATGGGCCTCGATCGCTAGCTGACCGACATC -3'
	5'-GATGTCGGTCAGCTAGCGATCGAGGCCCATGAGTTC -3'
Δ 131	5'-CCTCGGAACTCATGGGCTAAGATCGCGCCCTGACC -3'
	5'-GGTCAGGGCGCGATCTTAGCCCATGAGTTCCGAGG -3'

by sequencing at the University of Minnesota Microchemical facility. The oligonucleotides used to introduce the mutations to the MMOB gene are shown in Table 1.

Steady-State Kinetics Measurements. Steady-state kinetics experiments were performed using a Hewlett-Packard 8453 UV−vis spectrophotometer. For the multiple turnover reaction with the substrate nitrobenzene, the reaction rates were monitored by the release of the product *p*-nitrophenol at 404 nm ($\epsilon = 15$ mM^{-1} cm^{-1}) or the consumption of NADH at 340 nm ($\epsilon = 6.24$ mM^{-1} cm^{-1}). In some cases, comparative studies were performed by measuring O_2 uptake using a Clark-type oxygen electrode.

EPR Measurements of the Mixed-Valent MMOH. The anaerobic complex of mixed-valent MMOH with MMOB was prepared as reported previously (*8*, *18*). The MMOB mutants were added to MMOH before the samples were reduced. Phenazine methosulfate was used as a redox mediator. The EPR measurements were performed using a Bruker Elexsys E500 spectrometer equipped with an Oxford ESR-910 liquid helium cryostat.

Transient Kinetics Experiments. Transient kinetics was performed using an Applied Photophysics SX.18MV stopped-flow spectrometer (Surry, U.K.). All stopped-flow experiments were conducted under pseudo-first-order, single-turnover conditions as reported previously (*9*, *33*). In all experiments, 50 mM MOPS buffer at pH 7.0 or 7.6 was used and the molar ratio of MMOB/MMOH (sites) was maintained at 1:1. The final concentrations of the MMOH (sites) and MMOB after mixing were 25 μM. The substrates methane or nitrobenzene were added in large excess over the enzyme in some experiments under the conditions listed in the text or figure captions. The single-turnover data were analyzed by fitting the time course to the sum of two or more exponentials using the nonlinear regression program KFIT as described earlier (*9*, *33*). For a series of irreversible first-order or pseudo-first-order reactions, the reciprocal relaxation times (RRTs) of the exponentials required to fit the data give the number of steps in the reaction series and their rate constants. However, the assignment of a specific rate constant to a specific step requires additional information such as the extinction coefficients of the intermediates and the amplitudes of the exponential phases. In the case of MMO the assignments have been made in previous studies (*9*). The dependence of the transient kinetics of the single-turnover cycle on pH was determined as previously reported (*34*).

Numerical Simulations. The time course of the single turnover with nitrobenzene monitored at 404 nm was simulated with the numerical integration program KSIM using a fitting procedure similar to that previously reported

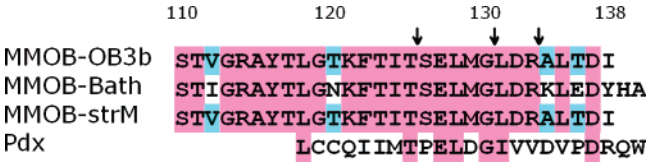

FIGURE 1: Alignment of C-terminal regions for MMOB from three different methanotrophs, *Methylococcus capsulatus* (Bath) (MMOB−Bath) (*48*), *Methylosinus trichosporium* OB3b (MMOB−OB3b) (*49*), and *Methylocystis sp*. strain M (MMOB−StrM) (*50*), and of putidaredoxin from the *Pseudomonas putida* $P450_{cam}$ system (Pdx) (*51*). The numbering system applies to MMOB−O3b. The arrows indicate where the mutations are made for the three C-terminal deleted mutants used in this study.

(*24*). The following mechanism was used in these simulations:

$$\text{nitrobenzene} + \mathbf{H}^{red} \xrightarrow{k_{HD}} \mathbf{O} \xrightarrow{k_{P*F}} \mathbf{P^*} \xrightarrow{k_{PF}} \mathbf{P} \xrightarrow{k_{PD}} \mathbf{Q} \xrightarrow{k_{QD}} \mathbf{T} \xrightarrow{k_{TD}} \mathbf{T1} \xrightarrow{k_{PR}} \mathbf{H}^{ox} + p\text{-nitrophenol}$$
$$\mathbf{P^*} \xrightarrow{k_{uncouple}} \mathbf{H}^{ox}$$

where **T1** is a product complex with a minor structural change from intermediate **T** that has a slightly different extinction coefficient. The $k_{uncouple}$ reaction is required to account for the less than 100% yield observed for some of the reactions utilizing MMOB mutants. Most of the rate constants used in simulations were based on the values published previously (see Table 3) (*9*, *24*, *33*, *35*) or determined in the current study. For unknown rate constants, manual iterations were performed to obtain the best fit to the data. The extinction coefficients of the species when nitrobenzene is the substrate were also determined in the same previous studies: **Q**, $\epsilon_{430} = 7500$ M^{-1} cm^{-1}; $\mathbf{H}^{ox}$ and **P**, $\epsilon_{430} = 2000$ M^{-1} cm^{-1}; **P***, $\epsilon_{430} = 750$ M^{-1} cm^{-1}; **O** and $\mathbf{H}^{red}$, $\epsilon_{430} = 1000$ M^{-1} cm^{-1}, **T**, $\epsilon_{430} = 6725$ M^{-1} cm^{-1}; **T1**, $\epsilon_{430} = 10\,000$ M^{-1} cm^{-1}; *p*-nitrophenol, $\epsilon_{430} = 10\,500$ M^{-1} cm^{-1}.

Product Distribution. The distribution of phenolic products from the MMOH catalyzed hydroxylation of nitrobenzene was determined by HPLC methods as previously described (*23*, *24*, *35*).

Determination of H_2O_2. The quantification of H_2O_2 released during partially uncoupled turnover was carried out using the method of Thurman et al. (*36*). The aerobic reaction of one or more of the sMMO system components with methane at the concentrations listed in Table 4 was initiated by the addition of 260 μM NADH in a 0.5 mL volume and quenched by the addition of the same volume of 3.5% trichloroacetic acid after 10 min. At this time, all of the NADH was oxidized. The precipitated proteins were removed by centrifugation. Then 200 μL of 10 mM ferrous ammonium sulfate and 100 μL of 2.5 M potassium thiocyanate were added to the supernatant. The red ferrithiocyanate complex was formed in the sample and was quantified at 480 nm using an experimentally determined extinction coefficient of $\epsilon = 90.9$ mM^{-1} cm^{-1}.

RESULTS

Activity of the C-Terminal Mutants. The C-terminal amino acid sequences for the best studied MMOB proteins are shown in Figure 1. The high degree of identity for this region among the proteins from different sources is consistent with a conserved function despite the lack of structure in solution.

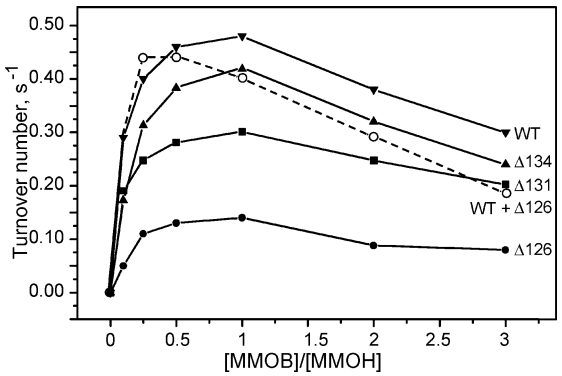

FIGURE 2: Effect of C-terminal MMOB mutants on steady-state activity: (▼) WT-MMOB; (▼) Δ134; (●) Δ126; (■) Δ131; (○) a 1:1 mixture of WT-MMOB and Δ126 plotted using the WT-MMOB/MMOH sites ratio. Reactions used nitrobenzene as a substrate and were monitored by the release of the product *p*-nitrophenol at 404 nm at room temperature. The concentrations of the reaction components are 1.0 μM MMOH (sites), 1.0 μM MMOR, 1.5 mM nitrobenzene, and 0.1 mM NADH in 50 mM MOPS, pH 7.6; $T = 25$ °C. The solid lines are designed to guide the eye; however the data can be simulated well on the basis of a model for the effect on steady-state kinetics of the complexes formed between the components as described in ref *18*.

This region is also largely absent in homologous regulatory components from related oxygenase systems, which are not functional when used in place of MMOB in the sMMO system, suggesting that it plays some specific role in methane oxidation. To determine whether this region is important for function, we constructed three deletion mutants: Δ126 (deleted last 13 residues 126−138, SELMGLDRALTDI), Δ131 (deleted last 8 residues 131−138, LDRALTDI), and Δ134 (deleted last 5 residues 134−138, ALTDI). CD spectra of these three mutants are identical to that of WT-MMOB in the spectral regions associated with specific types of secondary structure, suggesting that their structures are very similar and that the C-terminal region is, indeed, disordered in solution. When the mutants are used in activity assays based on product formation, the steady-state turnover numbers are lower than that found when WT-MMOB is used. However, turnover is not abolished as in the case of the N-terminal deletion mutant (*26*, *31*).[2] Use of Δ134 lowers activity slightly (~91% of WT), while Δ131 and Δ126 cause further reductions to ~63% and ~28% of WT, respectively. These differences are also reflected in the maximum turnover value shown for each mutant under the conditions used to obtain the data shown in Figure 2.

Origin of the Decreased Activity. One possible explanation for the decreased activity when the C-terminal mutants are used is a decreased affinity for MMOH such that the critical protein−protein complex is not saturated. This possibility can be explored by determining either the absolute effect of mutant concentration on the steady-state kinetics or the ability of the mutant to compete with WT-MMOB during turnover. As seen in Figure 2, a plot of the observed turnover number as a function of mutant MMOB concentration maximizes near 1:1 with the MMOH active site concentration for each of the mutants as observed for WT-MMOB. This suggests that a strong complex forms even at the relatively low concentrations used in steady-state assays. The decrease in the reaction rate at higher ratios of MMOB/MMOH is thought to result from the formation of other types of complexes that capture the sMMO components in unreactive forms (*18*). This is observed for the C-terminal mutants in much the same way as for WT-MMOB; thus these additional component complexes are apparently also formed by the mutants.

The ability of the C-terminal mutants to compete with WT-MMOB is also illustrated in Figure 2, dashed line. In this experiment, Δ126 MMOB and WT-MMOB were added together over a range of concentrations in a 1:1 ratio, and the data are plotted versus the WT-MMOB/MMOH ratio. If Δ126 were to bind much more weakly than WT-MMOB, then the plot would resemble that for WT-MMOB alone. In fact, a slightly higher rate is observed at less than stoichiometric WT-MMOB/MMOH concentrations because Δ126 is mildly activating and there are vacant MMOH sites for it to occupy. Near stoichiometric WT-MMOB/MMOH concentrations, the reaction is inhibited, presumably because Δ126 competes successfully with WT-MMOB for binding sites and the sites with Δ126 bound do not give as high a rate as those with WT-MMOB. Finally, at excess WT-MMOB to MMOH sites ratio, the rate is roughly the average of those expected using WT-MMOB and Δ126 separately, suggesting that the affinity of the two forms of MMOB for MMOH and in the inhibitory component complexes is similar.

Another possible reason for the lower observed maximum activity when using the mutants in the nitrobenzene assay is a change in the regioselectivity of hydroxylation to yield *m*- or *o*- rather then *p*-nitrophenol. These alternative products have much lower extinction coefficients in the 400 nm range, and distribution shifts of this type are caused by some other mutations in MMOB (*35*). However, HPLC analysis reveals a similar product distribution when using WT-MMOB and each of the mutant proteins (data not shown). Therefore, the lower activity observed here must be the result of less total product formed per second, indicating a decrease in flux through the catalytic cycle, partial uncoupling, or both. These aspects of the catalytic process are best-addressed using transient-kinetic approaches.

Transient Kinetics of ***Q*** *Formation and Decay Using C-terminal Mutants*. The time course for the formation and decay of intermediates **P** and **Q** in the absence of substrate can be conveniently monitored at 700 and 430 nm, respectively, as shown in Figure 3 (*24*, *34*, *37*). Multiple exponential fitting of the time courses, an example of which is shown in Figure 4, yields the rate constants of intermediate formation and decay.[3] The rate constants observed using WT-MMOB and the C-terminal deletion mutants are summarized in Table 2. If it is assumed that the larger rate constant observed for a two-exponential fit of the time course monitored at 430 nm is that for **Q** formation, then the mutants evoke at most 15% of the rate constant found when using WT-MMOB. However, this decreased rate constant for **Q**

[2] In the case of sMMO from *Methylosinus trichosporium* OB3b, about 0.5% of the maximal turnover number is observed without MMOB present (*8*), and this remains when MMOB without the N-terminal 29 residues is used in assays (*26*).

[3] Multiple exponential fitting directly yields relaxation times not rate constants. However, we have shown that the MMO catalytic cycle is described well as a series of irreversible first-order or pseudo-first-order steps, so the reciprocal relaxation times give rate constants for the steps (see Experimental Procedures) (*9*).

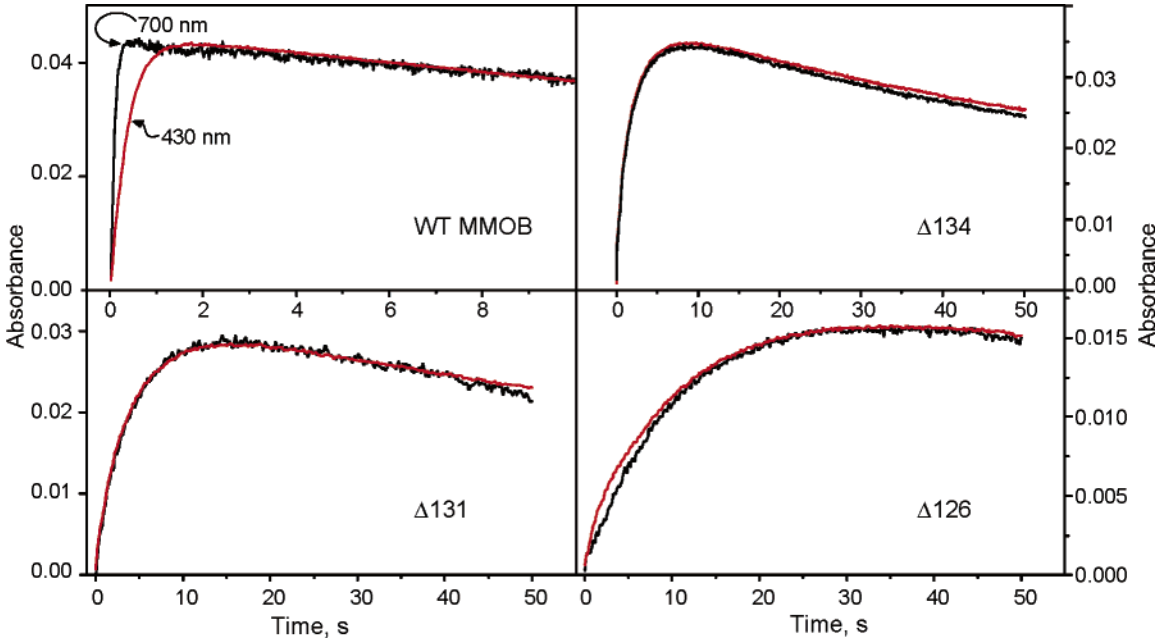

FIGURE 3: Time courses for reaction of diferrous MMOH with O_2 monitored at 430 nm (red) and 700 nm (black) at 4 °C in 50 mM MOPS, pH 7.0. One of the forms of MMOB was also present in equal concentration to MMOH (sites) for each experiment: (A) WT-MMOB; (B) Δ134; (C) Δ131; (D) Δ126. The absorbance scales pertain to the 430 nm data. The traces for 700 nm are enlarged to facilitate comparison.

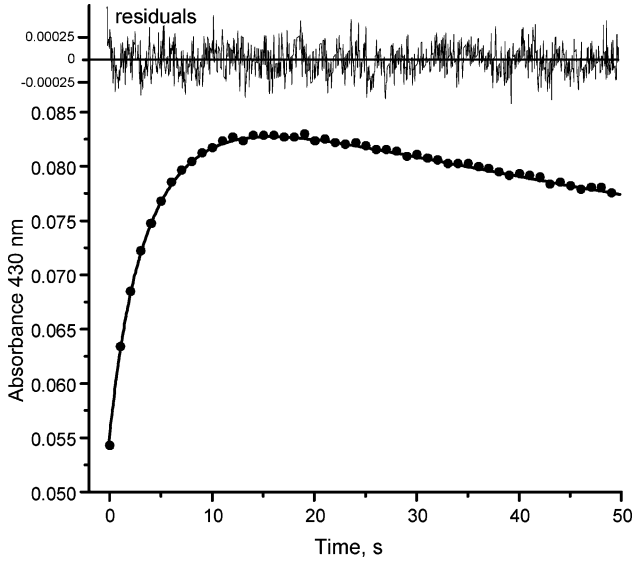

FIGURE 4: Multiple exponential fitting for the time course of the reaction using Δ131. The time course of the single-turnover reaction of reduced MMOH with O_2 in the presence of equimolar Δ131 at 4 °C, pH 7.0 (dots), was fit by two summed exponentials (solid line) (reciprocal relaxation time (fast) = 0.20 ± 0.03; reciprocal relaxation time (slow) = 0.009 ± 0.002). Every 20th point is shown for clarity. The residuals are shown at the top.

Table 2: Rate Constants for Single-Turnover Reactions with and without Substrate using C-Terminal Deletion MMOB Mutants[a]

sample	**P** formation k_{PF}, s^{-1}	**Q** formation k_{PD}, s^{-1}	**Q** decay k_{QD}, s^{-1}
WT-MMOB	10.2 ± 1.6	2.4 ± 0.1	0.04 ± 0.01
Δ134	0.34 ± 0.08	*b*	0.012 ± 0.003
Δ131	0.20 ± 0.03	*b*	0.009 ± 0.002
Δ126	0.042 ± 0.02	*b*	0.007 ± 0.002
WT-MMOB + CH_4	10.2 ± 1.6	2.4 ± 0.1	2.88 ± 0.12
WT-MMOB + CD_4	10.0 ± 1.6	2.4 ± 0.1	0.07 ± 0.01
Δ134 + CH_4	0.34 ± 0.08	*b*	0.22 ± 0.05
Δ134 + CD_4	0.30 ± 0.08	*b*	0.03 ± 0.01

[a] Conditions: pH 7.0, 4 °C, methane added at 200 μM when present. [b] Not resolved. It is likely that the **Q** formation rate constants are as fast as or faster than those observed using WT-MMOB.

formation could be caused by a change in either the **Q** formation step itself or one of the steps leading to an earlier intermediate, **O**, **P***, or **P**. In principle, this question can be readily addressed by comparing the time courses at 700 and 430 nm, but the analysis is complicated by the fact that **Q** also absorbs at 700 nm. In the case of single-turnover reactions run using WT-MMOB, the change at 700 nm is very fast compared with that at 430 nm, so the formation of **P** can be distinguished from the formation of **Q** (see Figure 3A). In the case of the reactions run using the mutant MMOBs, the very rapid change at 700 nm characteristic of **P** formation is not observed. Exponential fitting of the 700 nm time courses yields approximately the same set of rate constants as that observed for the 430 nm data. This suggests that the formation of **P** is very slow when the mutant MMOBs are used such that either **Q** or a mixture of **Q** and **P** arising effectively on the same time scale gives rise to the 700 nm absorbance. Accordingly, the rate constant that we obtained at 430 nm is an *apparent* **Q** formation rate and actually pertains to an earlier step. This suggests that the C-terminal region of MMOB is required to efficiently form either **P** or an earlier intermediate, that is, **O** or **P***. In addition, the **Q** autodecay rates decrease 2.5−6-fold with these mutants as shown in Table 2.

We have previously reported a similar decrease in the formation rate constants for **P** for the mutant H33A in the N-terminus of MMOB (*24*). The basis for the effect of H33A is unknown, but it was proposed that the histidine residue may play some role in the process of proton transfer, which is essential for the conversion of **P*** to **P**. Previous studies showed that with WT- MMOB, the rate constants for the **P** and **Q** formation reactions decrease as pH increases, while the **Q** decay rate constant is not affected by pH (*34*). Freeze quench experiments suggested that the **O** decay (**P*** forma-

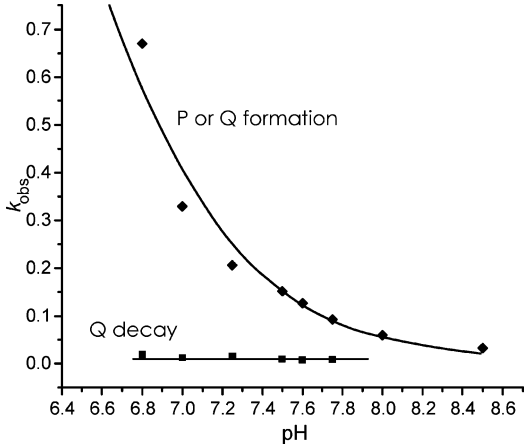

FIGURE 5: pH dependence of the observed rate constants in the time course for the reaction of diferrous MMOH with O_2 in the presence of Δ134 monitored at 430 nm. The solid line through the **P** or **Q** formation data is a fit using the Henderson−Hasselbach equation for a single ionization.

tion) reaction rate constant is also pH independent. A plot of the observed rate constants as a function of pH for the time course using the Δ134 mutant is shown in Figure 5. The faster rate constant exhibits strong pH dependence, while the slower one does not, consistent with the slower values being assigned to **Q** decay, as expected. Each C-terminal mutant gives a similar pH-dependent fast rate constant. The pK_a value (6.4) for the pH-dependent step of the Δ134 mutant affected reaction is slightly lower than that observed for **P** formation using WT-MMOB (pK_a = 7.5) (*34*). Nevertheless, if, as argued above, this step is not **Q** formation, then its pH dependence suggests that it is **P** formation because it is the only other known pH-dependent step. If this is the case, then use of the C-terminal MMOB mutants decrease the rate constant of **P** formation by at least 97%.

Transient Kinetics of Single Turnover Using Nitrobenzene as a Substrate. The effects of C-terminal deletion on the single-turnover kinetics of a reaction with a substrate present at 25 °C are illustrated in Figure 6A. A higher temperature is used for these experiments to allow better resolution of the slower steps and to permit comparison with room-temperature assays. Steps throughout the turnover cycle can be monitored at 430 nm using nitrobenzene as a substrate. One first observes the rapid formation and decay of **Q** leading to the weakly absorbing protonated *p*-nitrophenol bound in the hydrophobic active site at intermediate **T**. Then, the absorbance increases as *p*-nitrophenol is released and ionizes in solution to yield the strongly absorbing free product. Note the notch at about 0.25 s in the time course using WT-MMOB shown in Figure 6A due to the rapid formation of **Q**, slower decay of **Q**, and very slow decay of **T**. In contrast, no notch is observed for any of the time courses for reactions using the C-terminal deletion mutant MMOBs. Thus, the **Q** accumulation phase is not kinetically resolved, which is consistent with the conclusion from the lower temperature single-turnover experiment in the absence of substrate that slower **P** formation results in apparent slow formation of **Q**.

Although it is possible in principle to fit the complex reaction time courses shown in Figure 6A by multiple-exponential nonlinear regression techniques, we have found that a combination of nonlinear regression and numerical integration simulation gives a more reliable result (*24*). The

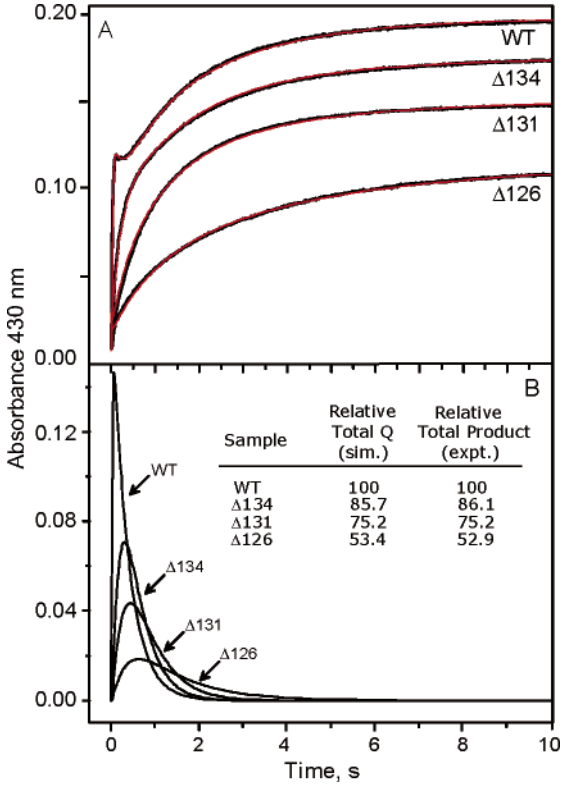

FIGURE 6: Time courses of single-turnover reactions with nitrobenzene as substrate. In panel A, the reactions were monitored by the release of the product *p*-nitrophenol at 430 nm at 25 °C with stopped-flow spectroscopy. Black traces are the experimental data, while the superimposed red curves are numerical integration simulations performed as described in Experimental Procedures. The rate constants used are given in Table 3, and the extinction coefficients for the species are given in Experimental Procedures. The final concentrations of the reaction components were 25 μM MMOH (sites), 25 μM MMOB, and 1.5 mM nitrobenzene in 50 mM MOPS, pH 7.6. Panel B shows a simulated time course of intermediate **Q** formation and decay based on rate constants derived from the fits for the time courses in panel A.

results of such fits are shown as red solid lines in Figure 6A and summarized in Table 3. In each case, adequate fits could be obtained by greatly decreasing the rate constant for **P** formation while leaving the constants for **Q** formation and **Q** and **T** decay nearly unchanged from those observed using WT-MMOB (a small decrease in **T** decay constant is required for the Δ126 mutant reaction). It is noteworthy that the decreased rate constant for **Q** decay observed in the absence of substrate is not observed when nitrobenzene is present. Thus, it appears that the major change in the kinetics of the MMOH catalytic cycle caused by the C-terminal deletions occurs in the formation of **P** irrespective of the presence or absence of substrate.

Evidence for Uncoupling. At the end of the single-turnover nitrobenzene oxidation reaction, **Q** is completely decayed, so all of the observed color is due to the *p*-nitrophenol product. The difference in the final absorbance for the reactions using different C-terminal mutants seen in Figure 6A shows that different amounts of product are formed, and thus the system is less well coupled when the mutants are used. Accordingly, the fits to the experimental data shown in Figure 6A (red lines) required a decrease in amplitudes for the exponential phases in addition to decreased rate constants for some of the phases. Lower product yield is

Table 3: Single-Turnover Nitrobenzene Oxidation by MMOH Using Mutant MMOBs[a]

sample	**P** formation k_{PF}, s^{-1}	**P** uncouple $k_{uncouple}$, s^{-1}	**Q** formation k_{PD}, s^{-1}	**Q** decay k_{QD}, s^{-1}	**T** decay k_{TD}, s^{-1}	**T1** decay k_{PR}, s^{-1}
WT-MMOB	>100	0[b]	55 ± 5	4.3 ± 0.5	1.5 ± 0.05	0.40 ± 0.05
Δ134	6.5 ± 0.6	1.1[b]	55 ± 10	4.3 ± 0.5	1.2 ± 0.05	0.40 ± 0.05
Δ131	2.2 ± 0.2	0.8[b]	55 ± 10	4.3 ± 0.5	1.5 ± 0.05	0.39 ± 0.05
Δ126	0.8 ± 0.1	0.7[b]	55 ± 10	3.3 ± 0.4	0.5 ± 0.05	0.16 ± 0.02

[a] Conditions: 1.5 mM nitrobenzene, pH 7.6, 25 °C. In all cases, $k_{HD} = 500\ s^{-1}$ and $k_{P*F} = 200\ s^{-1}$. The fit is not sensitive to these values because they are much faster than k_{PF}. [b] The ratio of the values for $k_{uncouple}$ and k_{PF} shown is fixed by the observed yield in the model used for the simulation (see Experimental Procedures) in which H_2O_2 is lost from **P***. Indistinguishable results are obtained by instead fixing the ratio of $k_{uncouple}$ and k_{PD} based on the observed yield. Thus, the step in which the uncoupling occurs cannot be unambiguously determined by the transient kinetic experiments alone.

Table 4: Peroxide Yield during Steady-State NADH Turnover by MMO System Components in the Presence of Methane[a]

system	H_2O_2 (μM)
MMOR + NADH	193
MMOR + MMOH + NADH	15
MMOR + MMOH + MMOB + NADH	24
MMOR + MMOH + Δ134 + NADH	32
MMOR + MMOH + Δ131 + NADH	36
MMOR + MMOH + Δ126 + NADH	39

[a] Component concentrations when present: MMOR, 2 μM; MMOB (or mutant), 20 μM; MMOH, 20 μM; NADH, 260 μM; 500 μM methane was present in all experiments. $T = 25$ °C.

one factor (in addition to the lower rate constant for product release in the case of Δ126) that contributes to the lower maximum turnover numbers exhibited by the system when the mutants are used in steady-state kinetic assays described in Figure 2.

The step in which uncoupling occurs can be determined by comparing the total amount of **Q** formed to the total product obtained at the end of the reaction. The simulated time courses for intermediate **Q** based on the fits to the data in Figure 6A are shown in Figure 6B. Integration of these simulated time courses gives the total **Q** formed. As seen from the inset table in Figure 6B, the amount of **Q** and the amount of product are correlated. Thus, uncoupling occurs at a step prior to **Q** formation. If it is assumed that one of these intermediates decays in part by a route that does not form **Q**, each of the reaction time courses can be simulated without changing the extinction coefficients of the intermediates. This accounts for the decrease in the exponential phase amplitudes for the fits to the time courses noted above.

The expected product of uncoupling at either the **P*** or **P** intermediate is H_2O_2. The formation and decay reactions of these intermediates are independent of substrate, so the colorimetric determination of H_2O_2 yield can be better evaluated using methane as the substrate because its product is nonchromophoric. As shown in Table 4, H_2O_2 is produced by the system during steady-state turnover of methane. However, the yield is difficult to accurately determine because MMOH is also an efficient catalase (*23*, *38*). A 10 min incubation was used to ensure that each reaction was complete. However, during this period, H_2O_2 is also converted to O_2 and water, so the values in Table 4 for reactions where MMOH is present should be considered the minimum peroxide yield. MMOR alone utilizes most of the electrons from NADH oxidation to form H_2O_2 from O_2 in the absence of MMOH. Addition of MMOH limits the H_2O_2 production by channeling the electrons into slow formation and decay of **Q**. When MMOB is present, the cycle greatly accelerates, and more H_2O_2 is formed due to uncoupling. Use of the mutant MMOBs causes the uncoupling to increase, maximizing when Δ126 is used.

Effects on Single Turnover with Methane as the Substrate. The effects of MMOB C-terminal deletion on the multiple and single-turnover reactions when methane is the substrate were investigated using the Δ134 mutant. The steady-state turnover number was essentially unchanged from that observed when WT-MMOB was used ($0.15 \pm 0.02\ s^{-1}$ at 4 °C). In contrast, the rate constants for specific non-rate-limiting steps in the catalytic cycle at 4 °C are significantly slowed as shown in Table 2. The **P** formation step is slowed to the same significant extent observed in the absence of substrate, consistent with the substrate-independent nature of the steps in the **Q** formation process. Interestingly, the **Q** decay rate, which can be easily determined by nonlinear regression fitting when the nonchromophoric methane to methanol reaction is used, is decreased about 10-fold compared to the reaction using WT-MMOB.

The decrease in **Q** decay rate constant is in sharp contrast with the nitrobenzene oxidation reaction described above in which no change in the **Q** decay rate constant occurred when the mutants were used. In the case of other types of MMOB mutants investigated previously, we have ascribed this unique behavior of reactions involving methane to a decrease in the quantum tunneling component of the reaction (*24*, *29*, *35*). Accordingly, it is observed that the deuterium KIE for the **Q** reaction with methane is decreased from about 40 to ~7 when WT-MMOB is replaced by Δ134 (Table 2). Most of this change (possibly all) is due to the decrease in the rate constant for the CH_4, rather than the CD_4, reaction. This is consistent with converting from a reaction dominated by tunneling to one exhibiting a primary KIE typically observed for an Arrhenius process. Thus, deletion of the MMOB C-terminus appears to have a significant effect on the nature of the reaction occurring in the MMOH active site.

Effects of C-Terminal MMOB Mutants on the Diiron Cluster Environment. Based on the kinetic results, the C-terminal region of MMOB is particularly important for the generation of the intermediate **P** form of the diiron cluster, which is located in the buried active site of MMOH. This suggests that the C-terminal region of MMOB interacts with the MMOH surface in such a way that structural changes can be transmitted to the MMOH diiron cluster. To test this hypothesis, we prepared MMOB−MMOH complexes with MMOH in the EPR active $S = {}^1/_2$, Fe(II)−Fe(III) mixed-valent state. The EPR spectrum of this state is particularly sensitive to the environment and electronic properties of the cluster, and we have shown previously that

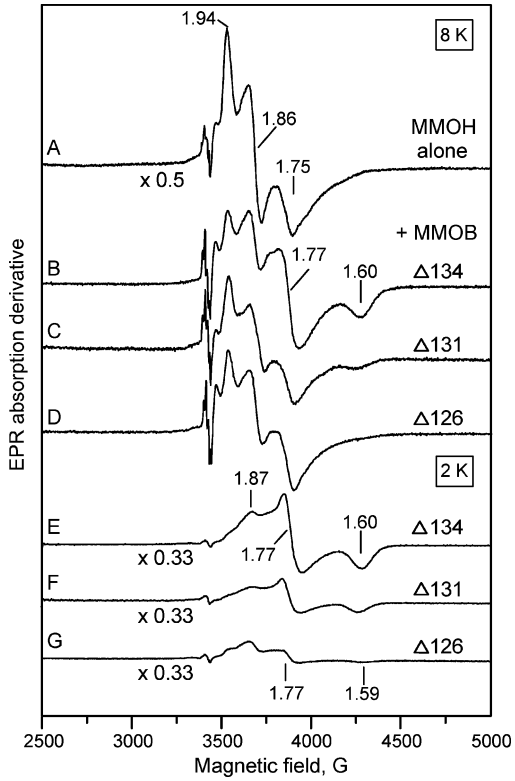

FIGURE 7: EPR spectra of the mixed-valent MMOH with MMOB and MMOB C-terminal deletion mutants at 8 and 2 K: (A) mixed-valent MMOH; (B) mixed-valent MMOH + Δ134, $T = 8$ K; (C) mixed-valent MMOH + Δ131, $T = 8$ K; (D) mixed-valent MMOH + Δ126, $T = 8$ K; (E, F, and G) the same samples as panels B, C, and D, respectively, recorded at $T = 2$ K. The concentration of MMOH (active sites) and MMOB (or mutant MMOB) when present were 400 and 300 μM, respectively. The spectra in panels B and E are indistinguishable from those of the equivalent MMOH−WT-MMOB complex. The spectrum shown in panel A is not detectable at 2 K under the conditions used due to saturation. The relevant *g*-values are marked. Instrumental parameters were as follows: microwave power = 2 mW at 9.6 GHz; modulation = 1 G at 100 kHz; gain = 5000. Samples were prepared as described in Experimental Procedures.

the environment changes dramatically when WT-MMOB is added (*12*, *18*, *19*). The EPR spectrum of the mixed-valent MMOB−MMOH complex ($g = 1.87$, 1.77, and 1.60) is readily resolved from that of mixed-valent MMOH alone ($g = 1.94$, 1.86, and 1.75) by lowering the sample temperature from 8 to 2 K, at which point the latter is easily saturated. The samples for the spectra in Figure 7 were prepared with a 3:4 ratio of MMOB to MMOH so that the spectra of both mixed-valent MMOH alone and the MMOB−MMOH complex can be observed at 8 K. Lowering the temperature to 2 K while maintaining relatively high microwave power results in the loss of only the signal due to mixed-valent MMOH alone (Figure 7E−G).

The spectra in Figure 7B−D show $g = 1.94$ resonances of approximately equal intensity. These signals are about one-fourth the intensity of the $g = 1.94$ resonance in the spectrum of mixed-valent MMOH alone. Thus, it appears that each of the mutant MMOBs binds essentially stoichiometrically to MMOH at the concentrations used for the EPR experiment, as expected from the results presented above. However, the progressive loss of the mixed-valent signal due to the complex as the length of the MMOB truncation increases was not expected. The samples contained the same amount of MMOH, and the same number of reducing equivalents were added. It is possible that the loss of the signal is due to a large increase in the coupling constant for the cluster in the complex, making it easier to saturate. If this were the case, however, a line shape change would be expected, and this is not observed. Similarly, a large increase in midpoint potential could have occurred to yield more MMOB−MMOH complex in the diferrous state, but this would also result in net oxidation of the mixed-valent MMOH fraction, which is not observed. We have observed a similar loss of the mixed-valent MMOH when MMOR is present (*39*). In that case, it was shown that the relative redox potentials of the two redox couples for the cluster exchanged such that the first electron is transferred at a lower potential than the second without a large change in the overall midpoint potential. Consequently, the cluster was found primarily in the diferric and diferrous forms. This may also be the case for the complexes with the truncated MMOB mutants. No matter what the cause, it appears that a significant change in the cluster environment occurs and that its extent depends on the length of the C-terminal truncation.

DISCUSSION

Oxygenase enzymes such as sMMO must generate very reactive oxidizing intermediates while at the same time restricting the reaction of these species to specific substrates. As a result, complex regulatory mechanisms have developed for both heme-based oxygenases such as cytochrome P450 and enzymes with non-heme metal centers such as sMMO. In most cases where more than one component is involved, regulation ensues from a protein−protein complex between a catalytic component and a regulatory component. In the case of MMO, this complex appears to allow exquisite control over (i) the size of the molecule that enters the active site, (ii) the regioselectivity of the reaction, (iii) the structure or environment of the MMOH active site metal cluster or both, and (iv) the degree of quantum tunneling involved in the C−H bond breaking process. Past studies have shown that many regions of the MMOB surface structure participate in regulation and that they alter different aspects of the process (*24*, *26*, *31*, *35*). These efforts have focused on the well-folded core region that regulates entry of substrates into the active site and the disordered N-terminal region, the deletion of which nearly terminates the oxygen activation steps in the reaction cycle. The present study shows that the disordered C-terminal region of MMOB also plays a unique role in regulation. Like the N-terminal region, it contributes to the oxygen activation process, but it is especially important for efficient coupling of reducing power to substrate oxidation. These aspects of sMMO regulation are discussed here.

Oxygen Activation Involving Proton Donation. As in the case of heme-containing oxygenases (*40*), O_2 activation in diiron oxygenases appears to involve formation and subsequent protonation of a peroxy intermediate (*9*, *16*, *34*). A similar hydroperoxy intermediate reacts directly with substrates in some types of enzymes such as flavo-oxygenases (*41*), but in the case of cytochrome P450 and MMO, the O−O bond cleavage to form a high-valent iron−oxo species occurs before the oxygenation reaction can occur with unactivated alkane substrates (*9*, *14*, *40*, *42*). Delivery of protons appears to be the key to this O−O bond cleaving process. In cytochrome P450, a proton delivery chain has

been identified from the protein surface to the bound oxygen (*43*). Such a pathway is not obvious in the structure of MMOH, although it has clearly not been eliminated as a possibility because the structure of the relevant MMOH−MMOB complex is not known. Based on kinetic solvent isotope effect (KSIE) studies, we have proposed that a solvent, perhaps bound to one of the irons of the cluster, is the direct proton source (*34*). However, the overall proton supply pathway might also involve active site solvents or amino acids from MMOH and MMOB that participate in non-rate-limiting steps.

The current results suggest that the C-terminal deletions greatly slow the step in which **P** is formed. As an alternative, one of the preceding steps might be slowed, but this is made less likely by the observation that the rate constant for the affected step is pH-dependent. Past studies have demonstrated this to be true for only **P** and **Q** formation steps (*34*). Looking at this in a different way, the observed pH dependence shows that proton transfer still occurs when the C-terminus is deleted, although the rate of transfer must be significantly slowed. The KSIE studies for the reaction using WT-MMOB showed that the rate-limiting step involves a one proton "hop" from a donor with a pK_a of about 7.5. The 1 pH unit shift in the pK_a for the donor when the Δ134 mutant is used (Figure 5) and the structural changes noted for the MMOH−Δ126 and −Δ131 mixed-valent complexes (Figure 7) suggest that the environment of the donor is changed when the mutant MMOBs are used. This could account for the change in rate constant of **P** formation. On the other hand, deletion of the C-terminus may make proton transfer into the active site less efficient by removing or misorienting a critical residue in the transfer chain from bulk solution, thereby forcing the use of an alternative pathway. This, in turn, may shift the rate-limiting step to a different donor with a different pK_a. These possibilities can be addressed by detailed KSIE effect studies using the mutants, and this is in progress.

Because the rate constant for the **Q** formation step is also pH-dependent (*34*), one might expect this step to also slow when the mutant MMOBs are used. It is possible that this does occur, but the slowing is not enough to allow the step to become resolved from the **P** formation step. Indeed, simulations of the reaction time course allow a significant alteration in the **Q** formation rate constant without affecting the quality of the fit. It is also possible that the two proton transfers occur from different sources, only one of which is affected by the C-terminal deletions. The latter notion is supported by our previous observation that the **P** and **Q** formation steps are each affected by a different histidine residue in the MMOB N-terminal region (*24*).

Rate-Limiting Step. The current results show that the rate-limiting step in the generation of **Q** using the C-terminal deletion mutants is likely to be **P** formation rather than the usual **Q** formation (*9*). This differs from the reaction using N-terminal deleted MMOB where a step in the formation of **O**, presumably O_2 access to the diferrous cluster, is rate-limiting in the **Q** formation process. Thus, it appears that the C-terminal deletion mutants are able to increase access to the active site for O_2 (and substrates) in a manner similar to WT-MMOB. This indicates that regulating substrate access is not the role of the C-terminal region.

The results reported here show that the largest changes in rate constants caused by use of the mutant MMOBs occur in the central steps of the reaction cycle. Nevertheless, the slowest rate constant in the overall cycle remains that of the terminal product release step. The maximum observed rate when product formation is measured is determined by three aspects of the reaction: (i) the product release rate constant; (ii) the degree of uncoupling during the **P** or **Q** formation step; (iii) the strength of the MMOB−MMOH complex relative to the tendency of MMOB to form a nonproductive alternative complex with itself or another sMMO component. The current data show that the ability to form productive and inhibitory complexes is not perturbed in a way that significantly affects the maximum rate by the C-terminal deletion. On the other hand, in the case of the Δ126 mutant, uncoupling has as large an impact on the observed rate as the decrease in the rate constant for the rate-limiting step. Indeed, simply multiplying the relative product yield (Figure 6B) by the relative rate constant for product release (Table 3) approximately accounts for the decreased maximum rate (Figure 2).

Uncoupling. Uncoupling is a commonly encountered phenomenon in monooxygenase reactions that results in less product being formed than expected based on the utilization of reduced pyridine nucleotide. Often, either superoxide or hydrogen peroxide is released before the oxygen activation reaction is complete. This can occur from the oxygenase component at some stage of the oxygen activation process or from the reductase if electron transfer to the oxygenase is not efficient. Past studies with the sMMO isolated from *Mc. capsulatus* (Bath) have suggested that one role of the MMOB is to provide coupling between the reductase and MMOH, hence the name "coupling protein" applied to MMOB in that system (*44*, *45*). In the wild-type *Ms. trichosporium* OB3b sMMO, little coupling of this type is observed. Instead, the MMOB has been shown to act by allowing efficient binding of O_2 and then substrate in the active site, leading to its designation as the "gating protein" (*15*).

Our past studies have shown that the system is >90% coupled in a single turnover in the presence of all of the components (*15*). In this case, the slight uncoupling appeared to occur in either the **P** or **Q** formation steps as observed here for the C-terminal deletion mutants. However, the degree of uncoupling is much greater when the Δ126 mutant is used, increasing to nearly 50%, suggesting that a major function of the C-terminus is to ensure efficient coupling.

The mechanism of uncoupling cannot be determined unequivocally from the available data. However, one possibility is that H_2O_2 is lost from one of the two peroxo species of the reaction cycle, **P** or **P***. Under this scenario, the yield would be determined by the fraction of **P*** or **P** that continues on to the next intermediate in the cycle. Similar considerations would apply to either intermediate, but H_2O_2 loss from **P*** is discussed here because its conversion to **P** is apparently the step most affected by the mutants. Accordingly, the values for $k_{uncouple}$ shown in Table 3 were calculated on the basis of the magnitude of the experimentally determined k_{PF} for **P** formation and the observed product yield for each mutant. These values were then shown to reproduce the experimental time course of nitrobenzene oxidation when used in a simulation. Surprisingly, this assumption results in very similar values for $k_{uncouple}$ for each mutant MMOB reaction. This suggests that the uncoupling reaction may be

a natural consequence of the structure of **P*** rather than a direct effect of the mutant. Interpreted in this way, the degree of coupling simply depends on the ability of MMOB to speed the formation of intermediate **P** so that there is less time for loss of peroxide from **P*** in a fixed rate reaction. This is a reasonable way to account for the high yield observed when using WT-MMOB because the **P*** to **P** reaction is very fast in this case.

Structural changes near the active site cluster induced by correct association of the C-terminal region of MMOB with MMOH are likely to be the underlying cause of the change in rate of **P*** to **P**. This is supported by the observation of unique changes in electronic properties of the diiron cluster as the mutant MMOB−MMOH complex forms, as well as apparent changes in the degree of quantum tunneling in the reaction of methane with **Q** that have been ascribed in past studies to changes in the active site structure.

Comparison with Regulation in P450$_{cam}$. One of the original experiments that indicated an effector function for one of the non-active-site-bearing components of monooxygenases showed that removal of the C-terminal tryptophan of putidaredoxin (Pdx) decreased the cytochrome P450$_{cam}$ turnover number by 1000-fold (*46*). It can be seen in Figure 1 that there is a surprising degree of sequence identity in the MMOB and Pdx C-terminal regions, although low similarity is found in the nonidentical residues. Pdx supplies both electrons required by P450$_{cam}$ for catalysis, but the nature of the individual electron transfers is different. The first electron needed to form the oxy complex can be supplied by many nonspecific donors. In contrast, the second electron needed to form the activated Fe(IV)−π cation radical species, which is believed to be the reactive equivalent of **Q** in sMMO, can only be efficiently supplied by Pdx (*47*). This suggests that the latter function involves specific protein−protein interactions and conformational changes needed to form the activated oxygen intermediate. It is conceivable that this is a common aspect of monooxygenase catalysis. However, the specific means by which the effector proteins perform this function remains a key unresolved question in each of the well-studied heme and non-heme systems. The studies presented here, in combination with our past studies, help to address this problem by first showing that all three of the major structural regions of MMOB are important in the regulation of monooxygenase catalysis and then defining discrete roles for each region in this complex process.

REFERENCES

1. Dalton, H. (1980) Oxidation of hydrocarbons by methane monooxygenase from a variety of microbes, *Adv. Appl. Microbiol. 26*, 71−87.
2. Leak, D. J., and Dalton, H. (1987) Studies on the regioselectivity and stereoselectivity of the soluble methane monooxygenase from *Methylococcus capsulatus* (Bath), *Biocatalysis 1*, 23−36.
3. Green, J., and Dalton, H. (1989) Substrate specificity of soluble methane monooxygenase. Mechanistic implications, *J. Biol. Chem. 264*, 17698−17703.
4. Wallar, B. J., and Lipscomb, J. D. (1996) Dioxygen activation by enzymes containing binuclear non-heme iron clusters, *Chem. Rev. 96*, 2625−2657.
5. Feig, A. L., and Lippard, S. J. (1994) Reactions of non-heme iron(II) centers with dioxygen in biology and chemistry, *Chem. Rev. 94*, 759−805.
6. Merkx, M., Kopp, D. A., Sazinsky, M. H., Blazyk, J. L., Muller, J., and Lippard, S. J. (2001) Dioxygen activation and methane hydroxylation by soluble methane monooxygenase: a tale of two irons and three proteins, *Angew. Chem., Int. Ed. 40*, 2782−2807.
7. Brazeau, B. J., and Lipscomb, J. D. (2000) Electron transfer and radical forming reactions of methane monooxygenase, *Subcell. Biochem. 35*, 233−277.
8. Fox, B. G., Froland, W. A., Dege, J. E., and Lipscomb, J. D. (1989) Methane monooxygenase from *Methylosinus trichosporium* OB3b. Purification and properties of a three-component system with high specific activity from a type II methanotroph, *J. Biol. Chem. 264*, 10023−10033.
9. Lee, S.-K., Nesheim, J. C., and Lipscomb, J. D. (1993) Transient intermediates of the methane monooxygenase catalytic cycle, *J. Biol. Chem. 268*, 21569−21577.
10. Fox, B. G., Surerus, K. K., Münck, E., and Lipscomb, J. D. (1988) Evidence for a μ-oxo-bridged binuclear iron cluster in the hydroxylase component of methane monooxygenase. Mössbauer and EPR studies, *J. Biol. Chem. 263*, 10553−10556.
11. Fox, B. G., Borneman, J. G., Wackett, L. P., and Lipscomb, J. D. (1990) Haloalkene oxidation by the soluble methane monooxygenase from *Methylosinus trichosporium* OB3b: mechanistic and environmental implications, *Biochemistry 29*, 6419−6427.
12. Fox, B. G., Hendrich, M. P., Surerus, K. K., Andersson, K. K., Froland, W. A., Lipscomb, J. D., and Münck, E. (1993) Mössbauer, EPR, and ENDOR studies of the hydroxylase and reductase components of methane monooxygenase from *Methylosinus trichosporium* OB3b, *J. Am. Chem. Soc. 115*, 3688−3701.
13. DeWitt, J. G., Bentsen, J. G., Rosenzweig, A. C., Hedman, B., Green, J., Pilkington, S., Papaefthymiou, G. C., Dalton, H., Hodgson, K. O., and Lippard, S. J. (1991) X-ray absorption, Mössbauer, and EPR studies of the dinuclear iron center in the hydroxylase component of methane monooxygenase, *J. Am. Chem. Soc. 113*, 9219−9235.
14. Lee, S.-K., Fox, B. G., Froland, W. A., Lipscomb, J. D., and Münck, E. (1993) A transient intermediate of the methane monooxygenase catalytic cycle containing an $Fe^{IV}Fe^{IV}$ cluster, *J. Am. Chem. Soc. 115*, 6450−6451.
15. Liu, Y., Nesheim, J. C., Lee, S.-K., and Lipscomb, J. D. (1995) Gating effects of component B on oxygen activation by the methane monooxygenase hydroxylase component, *J. Biol. Chem. 270*, 24662−24665.
16. Liu, K. E., Valentine, A. M., Qiu, D., Edmondson, D. E., Appelman, E. H., Spiro, T. G., and Lippard, S. J. (1995) Characterization of a diiron(III) peroxo intermediate in the reaction cycle of methane monooxygenase hydroxylase from *Methylococcus capsulatus* (Bath), *J. Am. Chem. Soc. 117*, 4997−4998.
17. Shu, L., Nesheim, J. C., Kauffmann, K., Münck, E., Lipscomb, J. D., and Que, L., Jr. (1997) An $Fe(IV)_2O_2$ diamond core structure for the key intermediate Q of methane monooxygenase, *Science 275*, 515−518.
18. Fox, B. G., Liu, Y., Dege, J. E., and Lipscomb, J. D. (1991) Complex formation between the protein components of methane monooxygenase from *Methylosinus trichosporium* OB3b. Identification of sites of component interaction, *J. Biol. Chem. 266*, 540−550.
19. Pulver, S. C., Froland, W. A., Lipscomb, J. D., and Solomon, E. I. (1997) Ligand field circular dichroism and magnetic circular dichroism studies of component B and substrate binding to the hydroxylase component of methane monooxygenase, *J. Am. Chem. Soc. 119*, 387−395.
20. Hendrich, M. P., Münck, E., Fox, B. G., and Lipscomb, J. D. (1990) Integer-spin EPR studies of the fully reduced methane monooxygenase hydroxylase component, *J. Am. Chem. Soc. 112*, 5861−5865.
21. Paulsen, K. E., Liu, Y., Fox, B. G., Lipscomb, J. D., Münck, E., and Stankovich, M. T. (1994) Oxidation−reduction potentials of the methane monooxygenase hydroxylase component from Methylosinus trichosporium OB3b, *Biochemistry 33*, 713−722.
22. Liu, K. E., and Lippard, S. J. (1991) Redox properties of the hydroxylase component of methane monooxygenase from *Methylococcus capsulatus* (Bath). Effects of protein B, reductase, and substrate, *J. Biol. Chem. 266*, 12836−12839.
23. Froland, W. A., Andersson, K. K., Lee, S.-K., Liu, Y., and Lipscomb, J. D. (1992) Methane monooxygenase component B and reductase alter the regioselectivity of the hydroxylase component-catalyzed reactions. A novel role for protein−protein interactions in an oxygenase mechanism, *J. Biol. Chem. 267*, 17588−17597.

24. Wallar, B. J., and Lipscomb, J. D. (2001) Methane monooxygenase component B mutants alter the kinetics of steps throughout the catalytic cycle, *Biochemistry 40*, 2220−2233.
25. Chang, S. L., Wallar, B. J., Lipscomb, J. D., and Mayo, K. H. (1999) Solution structure of component B from methane monooxygenase derived through heteronuclear NMR and molecular modeling, *Biochemistry 38*, 5799−5812.
26. Chang, S. L., Wallar, B. J., Lipscomb, J. D., and Mayo, K. H. (2001) Residues in *Methylosinus* trichosporium OB3b methane monooxygenase component B involved in molecular interactions with reduced- and oxidized-hydroxylase component: a role for the N-terminus, *Biochemistry 40*, 9539−9551.
27. Walters, K. J., Gassner, G. T., Lippard, S. J., and Wagner, G. (1999) Structure of the soluble methane monooxygenase regulatory protein B, *Proc. Natl. Acad. Sci. U.S.A. 96*, 7877−7882.
28. Nesheim, J. C., and Lipscomb, J. D. (1996) Large isotope effects in methane oxidation catalyzed by methane monooxygenase: evidence for C−H bond cleavage in a reaction cycle intermediate, *Biochemistry 35*, 10240−10247.
29. Brazeau, B. J., Wallar, B. J., and Lipscomb, J. D. (2001) Unmasking of deuterium kinetic isotope effects on the methane monooxygenase compound Q reaction by site-directed mutagenesis of component B, *J. Am. Chem. Soc. 123*, 10421−10422.
30. Lloyd, J. S., Bhambra, A., Murrell, J. C., and Dalton, H. (1997) Inactivation of the regulatory protein B of soluble methane monooxygenase from *Methylococcus capsulatus* (Bath) by proteolysis can be overcome by a Gly to Gln modification, *Eur. J. Biochem. 248*, 72−79.
31. Callaghan, A. J., Smith, T. J., Slade, S. E., and Dalton, H. (2002) Residues near the N-terminus of protein B control autocatalytic proteolysis and the activity of soluble methane monooxygenase, *Eur. J. Biochem. 269*, 1835−1843.
32. Fox, B. G., Froland, W. A., Jollie, D. R., and Lipscomb, J. D. (1990) Methane monooxygenase from *Methylosinus trichosporium* OB3b, *Methods Enzymol. 188*, 191−202.
33. Brazeau, B. J., and Lipscomb, J. D. (2000) Kinetics and activation thermodynamics of methane monooxygenase compound Q formation and reaction with substrates, *Biochemistry 39*, 13503−13515.
34. Lee, S.-K., and Lipscomb, J. D. (1999) Oxygen activation catalyzed by methane monooxygenase hydroxylase component: proton delivery during the O−O bond cleavage steps, *Biochemistry 38*, 4423−4432.
35. Brazeau, B. J., and Lipscomb, J. D. (2003) Key amino acid residues in the regulation of soluble methane monooxygenase catalysis by component B, *Biochemistry 42*, 5618−5631.
36. Thurman, R. G., Ley, H. G., and Scholz, R. (1972) Hepatic microsomal ethanol oxidation: Hydrogen peroxide formation and the role of catalase, *Eur. J. Biochem. 25*, 420−430.
37. Liu, K. E., Wang, D., Huynh, B. H., Edmondson, D. E., Salifoglou, A., and Lippard, S. J. (1994) Spectroscopic detection of intermediates in the reaction of dioxygen with the reduced methane monooxygenase hydroxylase from *Methylococcus capsulatus* (Bath), *J. Am. Chem. Soc. 116*, 7465−7466.
38. Andersson, K. K., Froland, W. A., Lee, S.-K., and Lipscomb, J. D. (1991) Dioxygen independent oxygenation of hydrocarbons by methane monooxygenase hydroxylase component, *New J. Chem. 15*, 411−415.
39. Liu, Y., Nesheim, J. C., Paulsen, K. E., Stankovich, M. T., and Lipscomb, J. D. (1997) Roles of the methane monooxygenase reductase component in the regulation of catalysis, *Biochemistry 36*, 5223−5233.
40. Davydov, R., Makris, T. M., Kofman, V., Werst, D. E., Sligar, S. G., and Hoffman, B. M. (2001) Hydroxylation of camphor by reduced oxy-cytochrome $P450_{cam}$: Mechanistic implications of EPR and ENDOR studies of catalytic intermediates in native and mutant enzymes, *J. Am. Chem. Soc. 123*, 1403−1415.
41. Massey, V. (1994) Activation of molecular oxygen by flavins and flavoproteins, *J. Biol. Chem. 269*, 22459−22462.
42. McMurry, T. J., and Groves, J. T. (1986) Metalloporphyrin models for cytochrome P-450, in *Cytochrome P-450 Structure, Mechanism, and Biochemistry* (Ortiz de Montellano, P. R., Ed.) pp 1−28, Plenum Press, New York.
43. Gerber, N. C., and Sligar, S. G. (1994) A role for Asp-251 in cytochrome $P\text{-}450_{cam}$ oxygen activation, *J. Biol. Chem. 269*, 4260−4266.
44. Green, J., and Dalton, H. (1985) Protein B of soluble methane monooxygenase from *Methylococcus capsulatus* (Bath). A novel regulatory protein of enzyme activity, *J. Biol. Chem. 260*, 15795−15801.
45. Gassner, G. T., and Lippard, S. J. (1999) Component interactions in the soluble methane monooxygenase system from *Methylococcus capsulatus* (Bath), *Biochemistry 38*, 12768−12785.
46. Sligar, S. G., Debrunner, P. G., Lipscomb, J. D., and Gunsalus, I. C. (1974) A role of the putidaredoxin COOH-terminus in $P\text{-}450_{cam}$ (cytochrome *m*) hydroxylations, *Proc. Natl. Acad. Sci. U.S.A. 71*, 3906−3910.
47. Tyson, C. A., Lipscomb, J. D., and Gunsalus, I. C. (1972) The roles of putidaredoxin and P450 complexes in methylene hydroxylation, *J. Biol. Chem. 247*, 5777−5784.
48. Stainthorpe, A. C., Murrell, J. C., Salmond, G. P., Dalton, H., and Lees, V. (1989) Molecular analysis of methane monooxygenase from *Methylococcus capsulatus* (Bath), *Arch. Microbiol. 152*, 154−159.
49. Cardy, D. L., Laidler, V., Salmond, G. P., and Murrell, J. C. (1991) Molecular analysis of the methane monooxygenase (MMO) gene cluster of *Methylosinus trichosporium* OB3b, *Mol. Microbiol. 5*, 335−342.
50. McDonald, I. R., Uchiyama, H., Kambe, S., Yagi, O., and Murrell, J. C. (1997) The soluble methane monooxygenase gene cluster of the trichloroethylene-degrading methanotroph *Methylocystis* sp. strain M, *Appl. Environ. Microbiol. 63*, 1898−1904.
51. Peterson, J. A., Lorence, M. C., and Amarneh, B. (1990) Putidaredoxin reductase and putidaredoxin. Cloning, sequence determination, and heterologous expression of the proteins, *J. Biol. Chem. 265*, 6066−6073.

BI051721J